Sulfur deficiency in iron pyrite (FeS_{2-x}) and its consequences for band-structure models

M. Birkholz, S. Fiechter, A. Hartmann, and H. Tributsch
Bereich Photochemische Energieumwandlung, Abteilungen Solare Energetik und Materialforschung, Hahn-Meitner-Institut, D-1000 Berlin 39, Federal Republic of Germany
(Received 31 October 1990)

The nature of the sulfur deficit in pyrite, as found before by chemical analysis and density measurements, has been investigated by powder x-ray diffraction (XRD). Structure-factor refinements showed that the sulfur population parameter deviates several percent from unity, although the cubic-unit-cell edge a only varies in the order of 10^{-3} Å. To do these high-precision a measurements, a determination of the Cu $K\alpha_2$ wavelength is made. Vegard's rule for sulfur-deficient pyrite is presented. The sulfur deficit is explained as a simple Schottky defect, whose vacancy-formation energy is about 0.3 eV. On the basis of ligand-field- and molecular-orbital-theory considerations, the band-structure model of pyrite is modified due to the presence of S vacancies. The most important electronic effect is the formation of defect states in the forbidden zone. This result will be discussed with respect to contradictory measurements concerning the electronic properties of pyrite.

INTRODUCTION

Iron pyrite, with the ideal composition FeS_2, has gained interest as a potential solar-cell material in recent years. Having a band-gap energy of approximately 0.95 eV, the efficiency for the conversion of solar radiation in a pyrite–p-n junction could theoretically reach about 20%. This would be less than for other materials having larger band gaps, however, nontoxic constituents, a high absorption coefficient ($\geq 10^5$ cm^{-1} for $h\nu > 1.3$ eV), and high quantum efficiencies ($>90\%$) (Ref. 1) could make pyrite a viable alternative for thin-film solar cells.

Many investigations with synthetic pyrite have already been done on single crystals grown by chemical vapor transport[2,3] (CVT) and thin films produced by metal organic chemical vapor-deposition[4] (MOCVD), chemical spray pyrolysis[5] (CSP), sulfurization of iron oxides[6] (SIO), and plasma-assisted sulfurization of thin iron films.[7] But to produce a good solar cell severe problems have to be overcome with pyrite that were uncovered in photoelectrochemical cells. Open-circuit voltages, V_{oc}, of n-type crystals were only found in the range 0.15–0.2 V,[1,8,9] and never reached a value of half the band gap or more, as is usual for semiconductors in electrochemical cells.[10] Since solar-cell efficiencies are linearly dependent on V_{oc}, this effect has to be understood.

The consistency with which low open-circuit voltages were measured raised the question of whether it would be due to an intrinsic defect, i.e., an electronic defect coupled to the material. This hypothesis gained importance as investigations by inductively coupled plasma with atomic emission spectroscopy (ICPAES) revealed that natural and synthetic crystals were found to be exclusively sulfur deficient, so pyrite would more appropriately be expressed as FeS_{2-x} rather than FeS_2, with x ranging between 0.05 and 0.25.[11,12] However, by the ICPAES method nothing can be said about the structural organization of the defects.

The aim of this work therefore was to understand the structure of the sulfur deficit in pyrite and to modify the electronic band-structure models that were all derived for ideal stoichiometric FeS_2.[1,13–16] The method used for the investigation of the defect structure was powder x-ray diffraction (XRD), which is adequate to detect nonstoichiometries in the range of several percent. Since RuS_2, known as the mineral laurite and isostructural to pyrite, did not show deviations from stoichiometry,[17] a RuS_2 powder was measured for comparison.

Pyrite crystallizes within the cubic space group $Pa\bar{3}$ (space group No. 205) with four formula units FeS_2 per unit cell ($a \approx 5.418$ Å), see Fig. 1. The local coordination of the iron atoms is sixfold and of the sulfur atoms is fourfold. Fe atoms are coordinated to six sulfur atoms, while those have bonds to three Fe and to one S atom. The local point-group symmetry for Fe is C_{4v} (trigonally distorted octahedral), but could be approximated for most considerations as O_h (octahedral), while for the sulfur atoms it is C_{3v} (tetrahedral). The iron atoms are arranged in a face-centered-cubic (fcc) sublattice in which the S atoms are embedded, occupying positions along the $\langle 111 \rangle$ directions. The 24 coordinates of the eight S atoms in the unit cells are described in $Pa\bar{3}$ by a single parameter u, so the positions of Fe and S atoms are as follows:

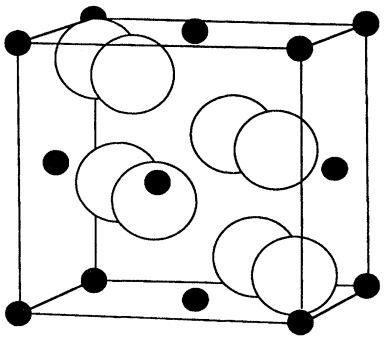

FIG. 1. Pyrite structure with black spheres representing Fe and white spheres S atoms. The unit cell indicated by the frame contains ideally four iron atoms and eight sulfur atoms.

Fe $0,0,0,\ 0,\frac{1}{2},\frac{1}{2}\ \ \frac{1}{2},\frac{1}{2},0\ \ \frac{1}{2},0,\frac{1}{2}$;

S $\pm(u,u,u\ \ u+\frac{1}{2},\frac{1}{2}-u,u\ \ -u,u+\frac{1}{2},\frac{1}{2}-u\ \ \frac{1}{2}-u,-u,u+\frac{1}{2})$.

u was found to be 0.385 04(5) (in fractional coordinates of the unit-cell length a).[18] An important detail of the ideal pyrite structure is that sulfur atoms are grouped as S_2 dimers. The dimers' centers of mass coincide with the positions of Cl atoms in the NaCl structure, so pyrite is sometimes compared with the NaCl structure when Fe atoms are imagined to occupy Na positions.

Ideal pyrite has an atomic ratio S:Fe=2:1 and a density of $\rho=5.01$ g/cm^3. Deviations from this ideality have been reported in the literature. In 1933, Buerger summarized the chemical analysis and density data obtained from natural samples. The atomic ratio quoted in this work ranged from 1.933 to 2.085.[19] Table I compares these and additional data from the literature with our own results gained on synthetic samples. The interpretation of these data is contradictory. Smith concludes that natural crystals with S:Fe ratios less than 2 have iron atoms residing on sulfur positions due to densities greater than the theoretical value of 5.01 g/cm^3 (Ref. 20) while the data of Juza, Biltz, and Meisel[21] and our own measurements[11,12] suggest missing S atoms in the lattice.

EXPERIMENTAL METHODS

Sample preparation

Pyrite single crystals were prepared by chemical vapor transport. 1–3 g of polycrystalline material and enough halogen to produce gas densities of 0.5–1.5 mg/cm^3 were sealed in cleaned and evacuated quartz ampules (diameter =22 mm, l=100–150 mm). The best transport conditions have been found with a temperature gradient of ΔT=970–850 K (for further details see Ref. 3). RuS_2 powder was synthesized from the elements in evacuated and sealed quartz sampules at 600 °C, yielding a fine purple-black powder.[22]

For XRD measurements as grown, pyrite powders were acquired from CERAC Inc. and partly heated in a vacuum of approximately 10^{-5} Torr. Pyrite CVT crystals were thoroughly mortared. To minimize falsification of integrated XRD intensities by texture-absorption effects, only those parts of the samples were used that passed through a 20-μm sieve.

TABLE I. Previously measured atomic ratios and densities of natural (nat.) and synthetic (syn.) pyrite samples.

Sample	Atomic ratio S:Fe	Density (g/cm^3)
Nat.(Colorado)[a]	1.994	
Nat. (Colorado)[a]	1.998	
Nat. (USA)[b]	1.95	4.978
Nat. (USA)[c]		4.951
Natural[d]	1.95	5.024
Natural[d]	2.01	5.005
Nat. (Murgul)[e]	1.91	4.92
Syn. (flux grown)[f]	1.995	
Syn. (flux grown)[f]	2.011	
Synthetic (CVT)[e]	1.93	4.973
Syn. (Cerac powder)[e]	1.95	4.981

[a]Reference 52.
[b]Reference 21.
[c]Reference 53.
[d]Reference 20.
[e]Reference 11.
[f]Reference 54.

XRD analysis—centroids of reflections

To evaluate the deviation from the ideal stoichiometry two sets of values have been extracted from XRD powder diffractograms: the centroids (centers of mass) of the reflections $2\theta_i$ and their relative intensities I_i.

Assuming that the environment of a vacancy is contracted compared to a normal atomic surrounding, the unit-cell length a should become a function of the deviation x from ideal stoichiometry (although nothing is said about the size of the contraction by this assumption). Because the scattering angle $2\theta_i$ of a Bragg reflection with Miller indices (hkl) depends on the mean value of the unit-cell edge $a(x)$ averaged over the whole powder, it will be shifted with the stoichiometry deviation of the sample. For cubic powders the scattering angle is given by the equation

$$\theta_i=\arcsin\left[\frac{\lambda(h^2+k^2+l^2)^{1/2}}{2a(x)}\right], \tag{1}$$

where λ is the wavelength of the used radiation. The larger the vacancy concentration the stronger the shift. If the dependency of unit-cell dimensions could be approximated by a linear function of the stoichiometry it follows the so-called Vegard's rule. For example, for cubic iron-monoxide $Fe_{1-x}O$, which appears in most cases to be iron deficient, Vegard's rule becomes $a=a_0-kx$, with $a_0=4.334$ Å and $k=0.489$ Å. (These are mean values from five papers, that are all listed in Ref. 23).

If pyrite occurs with variable chalcogen-content and this leads to a contraction of the unit cell, powders with different sulfur-to-iron-ratios should have different unit-cell edges. Therefore it should be possible to distinguish between samples having different S:Fe ratios by careful measurement of the lattice constant. Large differences in unit cell lengths were not expected, since the cyrstallographic hardness for pyrite is quite large (6.5 on Mohs's scale[24]), which would indicate a low flexibility of chemical bonds. Previously, only small variations of the lattice constant in the range from 5.407 to 5.428 Å have been reported.[18,25–30]

To measure the lattice constant very accurately the

TABLE II. Systematic errors $\Delta(\theta)$ for peak centroid measurements in powder diffractometry (after Ref. 31). Instrument parameters: diffractometer radius $R=200.5$ mm, axial beam divergence $\alpha=1°=0.001\,75$ rad, half horizontal beamwidth $h=5$ mm, Soller slit divergence $\Delta=2°$, $q=R\Delta/h$, and $Q_1=(1-\frac{1}{3}q+\frac{3}{8}q^2-\frac{1}{10}q^3)/(1-\frac{1}{6}q)$ and $Q_2=(\frac{1}{4}q^2-\frac{3}{40}q^3)/(1-\frac{1}{6}q)$.

j	Analytical form of $\Delta(\theta)_j$	Physical cause
1	c	constant misalignment
2	$-2b\cos\theta/R$	specimen surface displacement, b
3	$-\alpha^2\cot\theta/6$	flatness of sample
4	$\dfrac{-h^2[Q_1\cot 2\theta+Q_2\operatorname{cosec}2\theta]}{3R^2}$	axial divergence (one set of Soller slits)

analysis of diffractograms had to take systematic errors of the instrument and the measuring process into account. These 2θ-dependent systematic errors are very small (mrad) for a well-calibrated instrument, but for high-precision measurements, however, it is important to know that they could lead to incorrect unit-cell lengths in the range of a few per mill. To account for them a formula was derived by Wilson who set up a modified Bragg equation describing the shifting of XRD-reflection centroids caused by geometrical and physical abberations (those shifts are not to confuse with shifts due to stoichiometry variations).[31] In the case of cubic substances Wilson's formula becomes

$$\sin(\theta+\Sigma\Delta\theta_j)=\frac{\lambda(h^2+k^2+l^2)^{1/2}}{2a}\ . \tag{2}$$

$\Sigma\Delta(\theta)_j$ accounts for specimen displacement and equatorial and axial beam divergence as derived using Wilson's formula by inserting the values for diffractometer radius, slit settings, etc. Table II summarizes the four correction factors used for this work together with the instrument's constants (a more detailed description can be found in Ref. 32). Finally, the three parameters a (unit cell edge), b (specimen displacement), and c (constant misalignment of the instrument) were entered into the fit formula.

An equation according to Vegard's rule could not be formulated by measuring the lattice constants a of different powders alone, since data of the absolute S:Fe ratio are still missing.

XRD analysis—intensity of reflections

To obtain this stoichiometry coordinate a second type of evaluation of the powder diffractograms was made, performing a structure-factor refinement. In the case of a Schottky defect, the structure factor for sulfur-deficient pyrite is almost the same as for the stoichiometric compound, but the sulfur-scattering force for x-rays is reduced by a population parameter $P(\mathrm{S})$:

$$F(hkl)=4\left[\sigma_{hkl}f_{\mathrm{Fe}}+2P(\mathrm{S})f_{\mathrm{S}}\cos 2\pi\left[hu+\frac{h+k}{4}\right]\times\cos 2\pi\left[ku-\frac{k+l}{4}\right]\times\cos 2\pi\left[lu-\frac{h-l}{4}\right]\right] \tag{3}$$

with $P(\mathrm{S})\le 1$ for the compound FeS_{2P} $(2P=2-x)$. f_{Fe} and f_{S} are the temperature-dependent atomic-scattering factors for iron and sulfur, with isotropic temperature factors B_{Fe} and B_{S}. σ_{hkl} equals 1 only when all hkl are even or all odd, otherwise $\sigma=0$. From this it can be seen that reflections with mixed hkl are only due to the sulfur sublattice. Relative integrated intensities of XRD-powder reflections are proportional to $F^2=FF^*$, the 2θ-dependent Lorentz polarization factor L_P, and the multiplicity m of the reflection. Since in $Pa\bar{3}$ (hkl) indices are not, in general, cyclically permutable and since powder reflection positions are a function of the sometimes equivocal sum $h^2+k^2+l^2$, relative intensities were described by

$$I(hkl)=L_P(2\theta)\{m_1F(h_1k_1l_1)^2+m_1F(k_1h_1l_1)^2+m_2F(h_2k_2l_2)^2+m_2F(k_2h_2l_2)^2\}\ , \tag{4}$$

where $L_P(2\theta)$ and m_i are known for every reflection and F is dependent on both u and $P(\mathrm{S})$. Therefore the structure-factor refinement was reduced to a nonlinear regression of this sum. Fit values u, $P(\mathrm{S})$, a scaling factor SCF, and their standard deviations were calculated by the FORTRAN computer routines DRNLIN and DRSTAT from the *IMSL* library.[33]

MEASUREMENTS

All powder diffractograms were measured with a Siemens D500 diffractometer in the usual θ-2θ coupled mode. For the unit-cell determination Cu $K\alpha$ radiation (operating the anode with 45 kV and 30 mA), and for intensity measurements Mo $K\alpha$ radiation (45 kV, 40 mA)

were used. In the first case a graphite monochromator between sample and detector had to be used to reduce $K\beta$ and noncoherent scattered radiation, while this was done with a Zr band-edge filter for MoK radiation.

Changing to the Mo source for intensity measurements had a simple reason. The pyrite x-ray absorption for molybdenum radiation is smaller than for copper by almost a factor of 10 (Cu $K\alpha$: 955 cm^{-1}, Mo $K\alpha$: 115 cm^{-1}). It was shown that the interaction of crystalline size and absorption coefficient causes statistically strong variations in XRD reflection intensities.[34] This is easily understood as a texture effect (i.e., preferred orientation), where small ensembles of crystallites on the surface of the sample account for the main part of the reflection intensity. In Appendix A, it is shown that for Cu $K\alpha$ radiation and a 20-μm grain size pyrite powder 99.5% of the reflection intensity is due to the first layer of the sample (setting $2\theta=46°$ in this example). It is not very probable that the orientational distribution of this one polycrystalline layer is isotropic as it should be for the occurrence of correct relative intensities. For Mo $K\alpha$ radiation the penetration of the beam into the sample is almost ten times deeper and the XRD reflection's intensity exhibits a better mean value for a much bigger ensemble. To reduce statistical variations further the powder was passed through a 20-μm molecular sieve and throughout the measurement rotated (in the ϕ plane). With these constraints a mean deviation in diffraction intensities smaller than 2–3 % should be reliable.[34]

To maintain centroids and intensities from diffractograms, reflections were fitted with generalized Lorentz profiles (sometimes called regular Pearson VII), i.e., analytical functions of the form

$$I(2\theta_i)=\frac{I_0}{[1+k(2\theta_i-2\theta_0)^2]^m}\ , \tag{5}$$

with I_0, k, $2\theta_0$, and m being free-fit parameters. Computer programs to fit the measured reflections were part of the Siemens Diffrac 500 software package to run the x-ray diffractometer. In total 27 peaks were used to determine the unit-cell parameter a, and 23 peaks to determine P(S).

RESULTS

Determination of unit-cell lengths

Bragg reflections appeared in the measured diffractograms as α_1-α_2 doublets. As the number of fit parameters grow so do their errors. The first step in error reduction is accomplished by fitting profiles in a coupled mode, setting one centroid to be a function of the other,

$$\theta_2=\arcsin\left[\frac{\lambda_2}{\lambda_1}\sin\theta_1\right]\ , \tag{6}$$

where θ_k stands for the centroid of the α_k reflection ($k=1,2$). Using the wavelength measurements of Deslates, $\lambda(\alpha_2)/\lambda(\alpha_1)$ becomes 1.002 485.[35] Figure 2(a) shows the (620) reflection of CeO_2 powder fitted with generalized Lorentz functions and this quotient. It can be seen that the ratio does not fit the doublet well. To do high-precision work a new determination of the $\lambda(\alpha_2)/\lambda(\alpha_1)$ ratio was necessary. Therefore the CeO_2 (620) reflection was fitted in an uncoupled mode, leaving both centroids of the doublet as free-fit parameters. With the help of $\sin\theta_2/\sin\theta_1=\lambda(\alpha_2)/\lambda(\alpha_1)$, it follows that $\lambda(\alpha_2)/\lambda(\alpha_1)=1.002\,457(2)$, or in absolute units with the most recent value of Cu $K\alpha_1=1.540\,594\,6(11)$ (Ref. 36) $\lambda(\mathrm{Cu}K\alpha_2)=1.544\,388\,0(38)$ Å. From Fig. 2(b) it can be seen that the fit of the reflection with this wavelength ratio is much better. All the following fits of Cu $K\alpha$ doublets were done with this value.

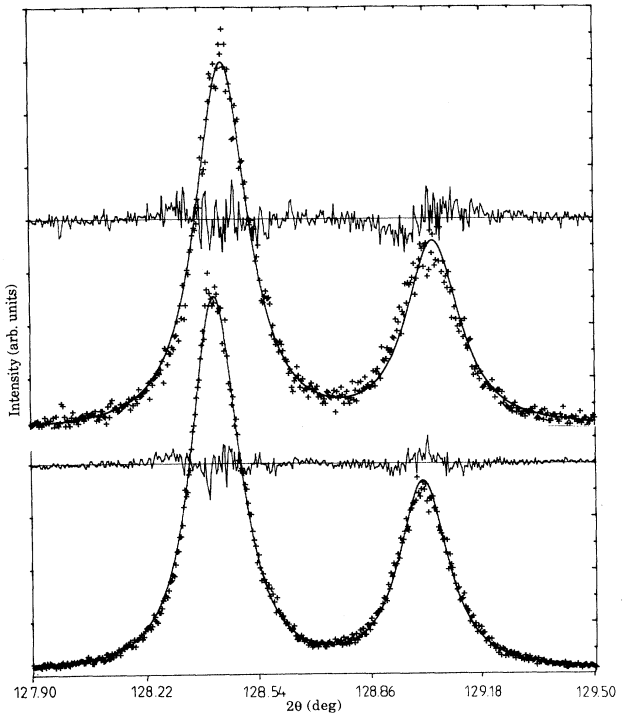

FIG. 2. NIST CeO_2(620) reflection for the precise determination of the Cu $K\lambda(\alpha_2)/\lambda(\alpha_1)$ ratio. The upper α_1-α_2 doublet (+, measured values) is fitted (−, fit curve) with the literature value, the lower with the determined $\lambda(\alpha_2)/\lambda(\alpha_1)$ ratio of 1.002 457(2). Also displayed are the difference curves. y, relative intensity (arb. units).

To evaluate to what precision a values could be determined with the Siemens D500 diffractometer and Wilson's formula, a standard had to be measured. For this purpose a CeO_2 sample was used, obtained from the U.S. National Institute for Science and Technology (NIST, former National Bureau of Standards). NIST specified the unit-cell length of the cubic CeO_2 powder to be (Certificate Standard Reference Material 674) $a=5.411\,29(8)$ Å for $T=(25\pm2)$ °C.

The linear thermal expansion coefficient for CeO_2 is $\alpha=10^{-5}°C^{-1}$,[37,38] so the variation of a in the specified temperature range would have been $\pm2.2\times10^{-4}$ Å. This uncertainty is bigger than the NIST-specified error, Δa,

and the unit-cell value would have been of more worth specifying a smaller temperature range. Measuring the NIST CeO_2 sample in a range from 45° to 145° yielded 14 reflections, which were fitted using the Wilson formula and the three fit parameters for $T=26.9(1)$ °C which resulted in $a=5.411\,26(16)$ Å, $b=-75(25)$ μm, and $c=-0.0011(15)°$. The error bars of this a value and the one from NIST overlap. The precision to which $\Delta a/a$ can be measured is concluded to be 3×10^{-5}.

Because the c value stands for the geometrical misalignment of the diffractometer it could be used as a fixed parameter for fittings of other data sets, provided the diffractometer was not rebuilt between both runs. With this procedure a values of pyrite powders were analyzed, fixing c to the constant value elucidated from the calibration measurement. In this way pyrite powders were analyzed with only two free-fit parameters: the unit-cell edge a and the horizontal displacement of the sample b.

Table III shows the results for ten different pyrite powders together with the temperature range in which the measurement was done. For reasons of clairity only a deviations from 5.4100 Å are displayed. The table will be interpreted as follows. (i) The cube edge a of pyrite is not a constant, but varies in the range of about 0.001 Å. This very small change justifies the use of the thorough Wilson formula and the precise determination of the Cu $K\alpha_2$ wavelength. Without them these small effects would have probably been hidden. (ii) Taking into account the linear thermal expansion coefficient of pyrite, $\alpha=8\times10^{-6}\,°C^{-1}$,[39] at the most a variations of 4×10^{-5} Å could have been expected within the temperature range of the measurements. The observed variations of a are larger by a factor of 20, hence thermal effects are not responsible for them and therefore can be neglected.

Structure factor refinements

Figure 3 shows a typical pyrite powder diffractogram measured with Mo K radiation. Employing the $\lambda(\alpha_2)/\lambda(\alpha_1)$ ratio, as found in the literature [1.006 049 (Ref. 35)], in combination with the absolute $\lambda(\alpha_1)$ value [0.708 866 062 Å (Ref. 36)] good results for reflection profile fits were obtained. Not all samples mentioned above were analyzed by structure-factor refinements, but only those with strongly differing a values. Isotropic temperature factors were not fitted but fixed to the best literature values[27] (i.e., those with the smallest errors), $B_{Fe}=0.208$ Å^{-2}, $B_S=0.253$ Å^{-2}, to reduce the number of variables. Table IV shows the output u and $P(S)$ parameters in addition to the R_w values of one intensity set for the total lattice and for the sulfur sublattice (for the latter only mixed hkl were summed), with

$$R_w=\left[\sum_{hkl}\frac{(I_{meas}-I_{fit})^2}{I_{meas}^2}\right]^{1/2}. \tag{7}$$

Also given are the data for a RuS_2 sample, for which fixed isotropic temperature factors B_{Ru} and B_S were taken from Ref. 40.

Table IV shows the most important result of this work: iron pyrite exhibits a sulfur deficiency in the few at % range. Except for one sample all powders had a sulfur deficit ranging up to 13 at. %, Sample CVT1002 gives $P(S)>1$, which does not make sense physically. The population value exceeds unity only by one standard deviation; this could indicate a statistical variation.

The table shows clearly that R_w values are much smaller for as-grown Cerac powders than for mortared CVT crystals. Relative faults in u and $P(S)$ are smaller, too. Although all samples were sieved to diameters smaller than 20 μm and measured with Mo radiation, the CERAC powders seem to be more unaffected by absorption and texture effects than powders of mortared CVT samples. Indeed, for an ensemble of 20-μm powder, still 50% of the integrated reflection intensity is due to the first two layers for typical scattering angles. The different R_w values therefore indicate that Cerac-pyrite powder has a smaller mean diameter than $\leq$20-μm CVT samples. This was also confirmed by optical inspection and elec-

TABLE III. Measured unit-cell edges a of different synthetic pyrite powders produced by chemical vapor transport (CVT) and purchased (Cer). (Only a deviations from 5.4100 Å are displayed.)

Sample	(a-5.41) (10^{-3} Å)	T (°C)	Preparation
CVT885	8.00(2)	27.0(2)	Br_2 transported
CVT991	8.02(3)	26.8(4)	Br_2 transported
CVT781	8.03(3)	27.1(5)	Br_2 transported
CVT990	8.05(4)	27.2(3)	Br_2 transported
CVT775	8.25(3)	27.4(4)	Br_2 transported
CVT957	8.34(4)	26.7(2)	Br_2 transported Ru-doped
H3Cer	8.36(2)	27.0(2)	Cerac powder (for 8 d heated at 120 °C)
HTCer1	8.38(3)	27.4(3)	Cerac-powder (for 14 h heated at 390 °C)
H2Cer	8.57(3)	27.0(2)	Cerac powder (not treated)
CVT1002	8.81(3)	27.4(3)	Br_2 transported

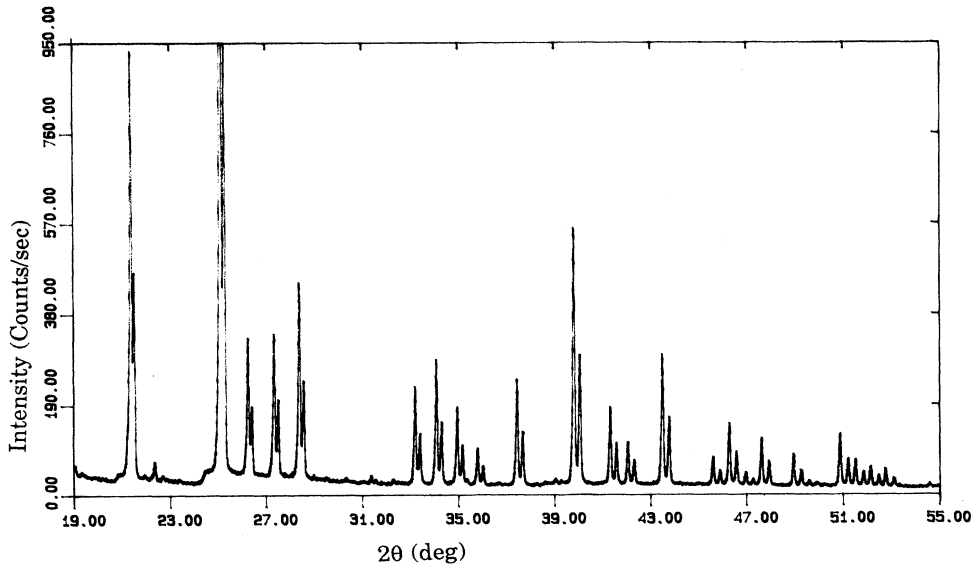

FIG. 3. Typical pyrite diffractogram measured with Mo $K\alpha$ radiation, for 2θ in the range 19–55°. The strongest (311) reflection has been cut to see details of smaller reflections.

tron microscopy. The structure-factor refinements of as-grown powders therefore are of higher reliability than those of mortared and sieved crystals.

Table IV also presents the results from the refinement of RuS_2 intensities. This compound crystallizes within the pyrite structure, too, and previous investigations do not indicate a chalcogen deficiency. The fit gives a sulfur population parameter to be very close to unity, with an accuracy one magnitude better than for the pyrite samples and a very small R_w value. Also, the sulfur positional parameter u has a higher accuracy than the value reported previously in the literature [$u=0.3885(7)$ after Ref. 40].

In thermodynamic equilibrium at temperature T the concentration of vacancies n/N (N being the number of all lattice sites, n the number of unoccupied positions) is described by a Boltzmann distribution with a vacancy formation energy H_f:

$$n/N=\exp(-H_f/kT)\ , \tag{8}$$

where k is Boltzmann's constant. All CVT pyrite samples were grown at a temperature of 853 K. Since the measured P(S) parameters and their errors are overlapping, it can not be excluded that H_f has the same value for all samples as expected when all were grown under the same conditions. But it cannot be excluded that the sulfur activity varied in the growth experiments influenced the crystals' final composition. Assuming that the crystals composition is mainly temperature dependent a mean vacancy formation energy of $H_{f,S}\approx 0.3$ eV is estimated by taking the mean P(S) value of the CVT samples (0.9825) for n/N and setting $T=853$ K. This value is quite low and for comparison it should be mentioned that the vacancy formation energy for anions in HgTe amounts to 0.65 eV.[41]

TABLE IV. Results of structure factor refinement in space group $Pa\bar{3}$.

Sample	Sulfur positional parameter $u(a)$	Sulfur population parameter P(S)	R_w (%) for the whole and for the S sublattice
CVT907	0.3886(12)	0.96(3)	7/13
CVT991	0.3878(13)	0.96(4)	7.4/11
CVT957	0.3889(13)	0.98(4)	7.4/14
H3Cer	0.3866(9)	0.87(2)	5.0/4.9
HTCer1	0.3855(5)	0.92(1)	2.9/3.2
H2Cer	0.3852(5)	0.95(1)	2.7/4.4
CVT1002	0.3878(9)	1.03(3)	5.1/11
RuS_2	0.3881(2)	1.002(5)	0.8/4.2

Vegard's rule

Figure 4 shows a plot of the unit cell a versus the population parameter $P(S)$. Because of the arguments mentioned above samples with R_w values larger than 5% were ignored. A linear fit of the data points gives a Vergard's rule relating the lattice constant and sulfur deficiency for FeS_{2-x}: $a(x)=a_0-kx$, where $a_0=5.4187(6)$ and $k=0.0015(6)$ Å. The k value is two orders of magnitude smaller than the one for nonstoichiometric iron monoxide. To enhance the accuracy of the constants the measurement of more data points with fewer texture-absorption effects would be necessary.

DISCUSSION

For iron pyrite a sulfur deficiency in the percent range was measured. The structure of the defect is proposed to be a simple Schottky defect with a vacancy formation energy of $H_{f,S}\approx 0.3$ eV. This picture is supported by positron lifetime measurements and investigations by transmission electron microscopy (TEM), the latter revealing a very good crystallinity of CVT crystals with no defect superstructure.[32] The observed vacancy concentration is comparable with stoichiometric deviations in iron oxides or iron monosulfide. It is interesting to note that the quantum efficiency for light-induced charge carrier excitation of pyrite is in the range of 0.9,[1] but for RuS_2 by a factor of 2–4 smaller,[17,42] although this work gave no hint for a sulfur deficit in the latter. Therefore it can be concluded that stoichiometric deviations do not necessarily induce a high concentration of recombination centers in these types of material.

In the following the effect of S vacancies for local atomic coordinations and for electronic band models will be discussed. Taking out a sulfur atom from the pyrite lattice results in the breaking of four bonds: one to the neighboring sulfur atom and three to Fe atoms. Because sulfur atoms are formally 1^- charged, producing a vacancy must be accompanied by leaving one minus charge behind to conserve charge neutrality. It is assumed that this electron is localized at the partner of the former S_2 dimer. By this mechanism, for every S vacancy another sulfur with a formal charge 2^- can be found that is only bound to three iron atoms. Such threefold coordinated, sp^3 hybridized S^2 atoms with a filled orbital directed into the fourth corner of the tetrahedron are already known in compound semiconductors, e.g., they are produced by metal vacancies in $CuInS_2$,[43] see Fig. 5. The point-group symmetry of these sulfur atoms remains the same as for all normal coordinated ones, C_{3v}.

We now consider the effects of sulfur vacancies on iron atoms. For this we assume the geometry of the coordinations to be more important than the S deficit induced occurence of S atoms formally charged 2^-, i.e., considerations of the charge of the ligands are neglected. Normally iron atoms are coordinated octahedrally to six sulfur atoms, the whole coordination sphere could be described as a FeS_6 molecule. If one takes away one corner from the bonding octahedron the local iron coordination becomes a FeS_5 molecule and the point-group symmetry of the coordination polyhedron will be reduced from O_h to C_4, see Fig. 6. Because no defect superstructure was observed[32] an homogeneous distribution of sulfur vacancies throughout the lattice is assumed. From this fact results a nonvanishing probability for some iron atoms to be not only fivefold, but even less coordinated (FeS_4, FeS_3 molecules, etc.). To calculate the frequencies of all disturbed coordinations a model is developed to describe the crystal as the sum of local coordinations (Appendix B).

The calculation shows that the concentration of affected iron coordinations amounts to a quarter of all irons for a typical sulfur deficit of 5% (i.e., $FeS_{1.9}$). Figure 6 shows the most frequent iron coordinations in sulfur deficient pyrite FeS_{2-x}, the octaheral FeS_6 and the tetragonal-pyramidal FeS_5 molecule with $3d$-orbital splitting due to ligand-field theory (LFT). For reasons of simplicity the S Schottky defect is assumed to be located on the z axis of the FeS_5 molecule. All orbitals with the z component (d_{xz}, d_{yz}, d_{z^2}) are then energetically more stabilized for the FeS_5 coordinations compared to the normal ones, since electrostatic forces between Fe $3d$ electrons and negatively charged ligands are reduced. In

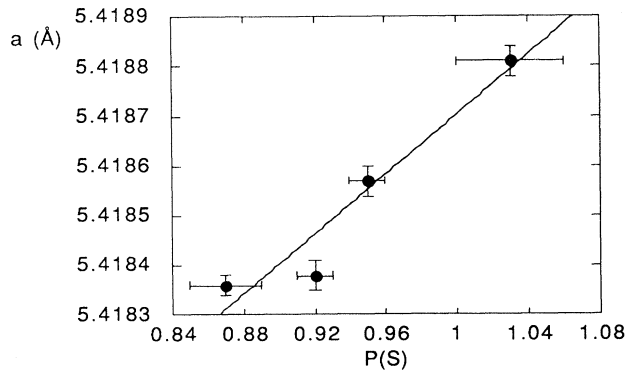

FIG. 4. Plot of the unit-cell length a/Å vs population parameters $P(S)$ for different pyrite powders. Only powders with R_w values smaller than 5% were considered. The constants in Vegard's rule $a(x)=a_0-kx$ for sulfur-deficient pyrite FeS_{2-x} are $a_0=5.4187(6)$ and $k=0.0015(6)$ Å.

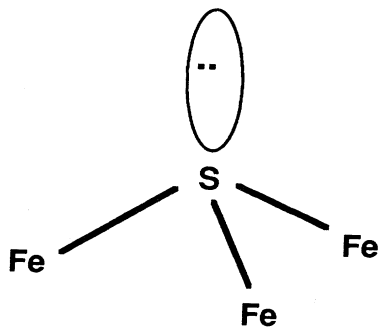

FIG. 5. Proposed defect coordination of S atoms that are neighbors of a vacancy. The two points in the ellipse indicate an orbital filled by two electrons.

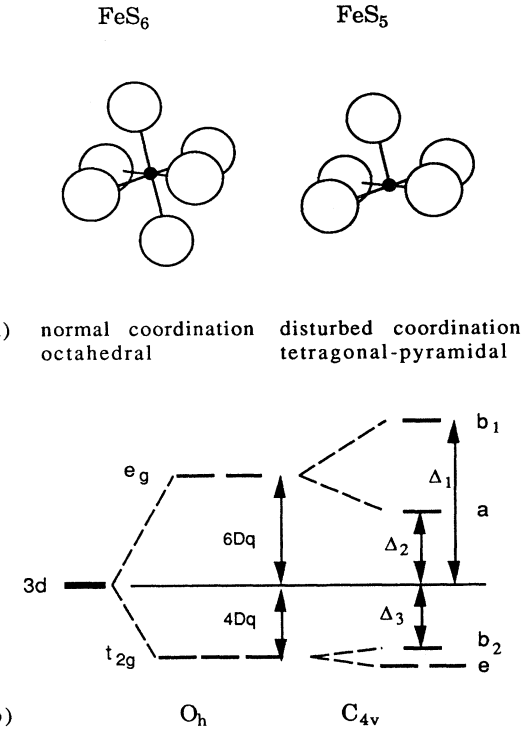

FIG. 6. (a) Most abundant local iron coordinations (FeS_6 and FeS_5 molecules) in sulfur-deficient pyrite FeS_{2-x}. (b) Splitting of Fe $3d$ orbitals in a field of octahedral (O_h) and of tetragonal-pyramidal (C_{4v}) symmetry due to ligand-field theory (LFT).

LFT the energetic displacements of $3d$ orbitals should cancel each other, thus, the relaxation of one e_g and two t_{2g} orbitals raises the energy of $d_{x^2-y^2}$ and d_{xy}. Most important is the electronic level that developed from the d_{z^2} state, named the a orbital in LFT nomenclature. The electron spins would remain paired for iron atoms only fivefold coordinated, which is consistent with magnetic measurements of pyrite, indicating only a small temperature-independent Van Vleck paramagnetism.[44]

In Fig. 7 a part of the band model for ideal stoichiometric pyrite is shown, first developed by Bither *et al.* by molecular-orbital considerations.[13] The antibonding orbitals constructed from Fe e_g and hybridized (S)sp^3 states are imagined as the conduction band in pyrite. The valence band results from overlapping of nonbonding Fe t_{2g} states. There is a wide consensus in the literature that this model describes the basic features of the band structure in pyrite. More sophisticated band-structure calculations were only more precise in that they could specify the amount of different atomic orbitals for every electronic band.[1,14–16]

Within the band-structure model of Bither *et al.* we now consider the effects caused by the sulfur deficit. It was shown above that only fivefold coordination of some of the iron atoms would lead to a splitting of e_g states, with the so-called Fe a state having a lower energy. Constructing an antibonding molecular orbital from this and from one of the sulfur states results in additional states (σ^* defect states) having an energy between conduction and valence band, see Fig. 7. Therefore, LF and MO theory predict the occurrence of defect states in the forbidden zone due to the sulfur deficit.

For stoichiometric deviations of some percent, the concentration of σ^* defect states would be of the order of 10^{21} cm^{-3}. Because of this high concentration it could be argued, that the density of states in the forbidden zone is so high that it could be assumed to combine to a defect band. The term "band" should only be used properly for energy levels with the periodicity of the crystal (that can be transformed into the Brillouin zone). Because there is no evidence for a defect superstructure, it should be used with care to describe the delocalization of defect states. But it is to be remembered that iron atoms are arranged in a fcc sublattice, in which every lattice point is surrounded from 12 neighboring (iron) atoms. For the case of 5% sulfur deficiency it was shown that approximately 25% of the iron coordinations would be affected. Therefore, three of twelve neighbors of an iron defect coordination are such defect coordinations, too. From this it is to be seen that for the case of some percent of

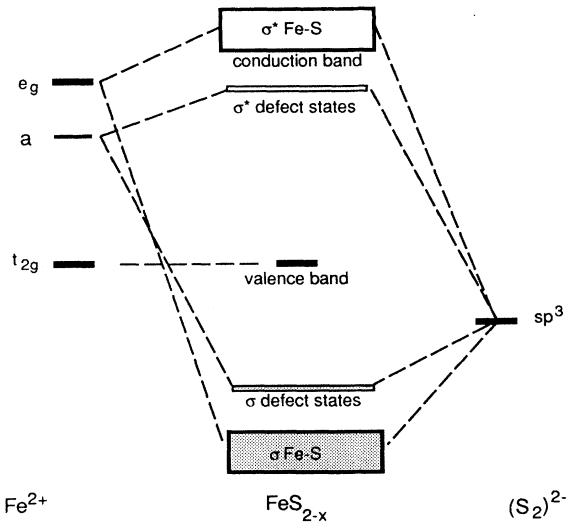

FIG. 7. Most prominent features of the band-structure model for pyrite with a sulfur deficit arranged as Schottky defects. For ideal stoichiometric FeS_2 ligand-field and molecular orbital theory predict Fe e_g and S sp^3 states to form bonding and antibonding orbitals. Bands are constructed by delocalization of those states through the whole crystal. The valence band is imagined to consist of nonbonding Fe t_{2g} states (Ref. 13). In FeS_{2-x} the normal atomic coordinations would contribute the most to the density of states (DOS) as above, but further states are introduced by some of the iron atoms, due to the S Schottky defects less than sixfold coordinated. Most important of them would be the a levels resulting from FeS_5 coordinations that combine with S sp^3 states to form antibonding orbitals with an energy lower than the conduction band of the ideal stoichiometric compound (σ^* defect states). Until now, nothing more could be said about the energetical position of these defect states and whether or not they would overlap with the conduction band (see text).

stoichiometric deviation there is a considerable overlap of σ^* defect states and the expression "defect band" could be used with some justification.

We can not *a priori* tell at what energy between the valence and conduction bands the defect band will be found and what width it will have. Two different situations are imaginable. First, the conduction and the defect band may be separated by a zone energetically forbidden for electrons. Second, both bands could have considerable width and may energetically overlap. Because the width of the defect band depends on the concentration of Fe *a* states, the band-gap energy would become a function of the stoichiometric deviation in both cases.

It is interesting to note, that the measured band-gap energies for pyrite vary in a wide range between 0.8 and 1.1 eV.[45–48] Also the open-circuit voltage, V_{oc}, obtained from a photoelectrochemical solar cell was less than half the band gap as is usual for other semiconductors. Therefore we propose to understand these unexplained electronical properties of pyrite in terms of defect states or a defect band due to the sulfur deficiency. This interpretation should be taken as a first working hypothesis. It is supported by luminescence measurements, previously taken in our laboratory at 10 K, that gave luminescence yields smaller than 10^{-7}, indicating a high concentration of states within the forbidden zone which mediate electron relaxation.[49] More experimental evidence for their existence came from magnetic susceptibility measurements that resulted in activation energies smaller than the optically observed band gap.[50] The authors explained this effect with defect states within the forbidden zone, too. It should be mentioned that the relatively high electron mobilities measured in pyrite (ranging from 100 to 2000 cm^2/Vs after Ref. 51) would not be easy to explain with the high concentration of defect states as proposed here. The question arises, how electrons should move in the conduction band when the probability is fairly high to be scattered from defect states.

Considering the electronic properties of pyrite it should be kept in mind that even more strongly disturbed iron coordinations (FeS_4, FeS_3 molecules, etc.) would be introduced by an homogeneous S vacancy distribution, see Appendix B. Electronically, these coordinations would lead to still stronger deviations from the normal Fe $3d$ splitting and to even more states within the forbidden zone. Because FeS_5 molecules are by far the most abundant defect coordinations it is assumed that to a first approximation they can account for the observed electronic effects that have not been explained until now. But it must be remembered that electronic states due to even more strongly disturbed iron coordinations remain to be incorporated in a more detailed model. The most important thing for optimizing pyrite as a solar-cell material will be to reduce the S vacancy concentration and to produce material having an S:Fe ratio very close to 2:1. This should be possible if the temperature dependence of the defect concentration is emphasized in subsequent works.

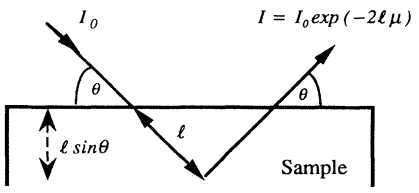

FIG. 8. Depth dependence of the reflected x-ray intensity.

ACKNOWLEDGMENTS

We like to thank Mike Fearheiley, Marinus Kunst, Stefan Seeger, and Greg Smestad for fruitful discussions and for careful reading of the manuscript.

APPENDIX A: DEPTH DEPENDENCE OF INTEGRATED X-RAY-REFLECTION INTENSITY

The absorption of x rays is described by the law of Lambert and Beer,

$$I = I_0 \exp(-2l\mu) , \tag{A1}$$

with I_0 the incident and I the damped intensity, $2l$ the path of the beam in the sample, and μ its absorption coefficient for the wavelength used, see Fig. 8. The total integrated x-ray intensity is proportional to the integration over I for all paths $2l$:

$$I_{int}(\infty) = I_0 \int_0^\infty \exp(-2l\mu) dl = \frac{I_0}{2\mu} . \tag{A2}$$

To calculate the integrated intensity caused by the sample down to a particular depth t_0, the integral is not to extend to infinity, but to l_0 with $l_0 = t_0/\sin\theta$ (see Fig. 8):

$$I_{int}(t_0) = \frac{I_0}{2\mu} \left[1 - \exp\left[-\frac{2\mu t_0}{\sin\theta} \right] \right] . \tag{A3}$$

The quotient

$$\frac{I_{int}(t_0)}{I_{int}(\infty)} = 1 - \exp\left[-\frac{2\mu t_0}{\sin\theta} \right] \tag{A4}$$

describes how much of the integrated intensity is caused by the reflection of powder layers down to the depth t_0. Inserting the x-ray-absorption coefficient for pyrite (Cu$K\alpha$: 955 cm^{-1}) and assuming the powder to be composed of crystallites with a diameter of 20 μm, it is calculated that 99.5% of the total intensity is due to the first layer of crystallites (for a typical scattering angle $\theta = 46°$). Only if those crystallites are random oriented (which is not very probable) correct x-ray intensities are measured. To reduce intensity variations due to preferred orientation (texture) the use of other x-ray wavelengths (for which the powder's absorption coefficient is smaller) is recommended, e.g., Mo$K\alpha$ with $\mu = 115$ cm^{-1}.

APPENDIX B: FREQUENCY OF DISTURBED COORDINATIONS IN FeS_{2-x}

Within the model explained in the following the crystal is cut into local atomic coordinations, assuming each to be a cell containing one molecule. In the case of ideal stoichiometric FeS_2 the unit cell (consisting of four formula units) would be composed of two different molecu-

TABLE V. Relative frequencies of normal and disturbed coordinations in $FeS_{1.90}$.

Local coordinations	n	Relative frequencies w_i	Number of Fe atoms	Number of S atoms
FeS_6	0	73.5%	0.735	4.41
FeS_5	1	23.2%	0.232	1.16
FeS_4	2	3.1%	0.031	0.12
FeS_3	3	0.2%	0.002	0.000
FeS_2	4	0.008%	0.000	0.000
S_2Fe_3	0	90.25%	2.71	1.805
SFe_3	1	9.5%	0.29	0.095
Σ		200%	4	$7.60=4\times1.90$

lar cells, one bonding octahedron around iron FeS_6, and another bonding tetrahedron around sulfur S_2Fe_3:

$$4FeS_2=FeS_6+S_2Fe_3 \ . \tag{B1}$$

Introducing homogeneously distributed S vacancies in the lattice results in the origin of FeS_5, FeS_4 coordinations, etc. The sulfur-deficient compound FeS_{2-x} then becomes the sum of all of them with frequencies $w_i(x)$:

$$FeS_{2-x}=w_0FeS_6+w_1FeS_5+w_2FeS_4 + \cdots w_7S_2Fe_3+w_8SFe_3 \ . \tag{B2}$$

The w_i will now be determined. The probability of finding a S atom at S-lattice site is $P(S)=(1-x/2)$ for FeS_{2-x}. The complementary probability $x/2$ describes how often a vacancy can be found. Fully octahedral coordinations around iron atoms therefore have the probability

$$w_0=\left[1-\frac{x}{2}\right]^6 , \tag{B3}$$

and an adequate expression for FeS_5 coordinations is

$$\left[\frac{x}{2}\right]\left[1-\frac{x}{2}\right]^5 . \tag{B4}$$

Because of combinatoric reasons there are six different octahedrons with one missing sulfur at a corner. Therefore the FeS_5 frequency in the lattice becomes

$$w_1=6\left[\frac{x}{2}\right]\left[1-\frac{x}{2}\right]^5 . \tag{B5}$$

Generally, the frequency of FeS_{6-n} coordinations is then

$$w_n=\begin{bmatrix}6\\n\end{bmatrix}\left[\frac{x}{2}\right]^n\left[1-\frac{x}{2}\right]^{6-n} . \tag{B6}$$

Applying the same considerations to $S_{2-m}Fe_3$ coordinations, the chemical formula for sulfur-deficient pyrite FeS_{2-x} in the molecular-cell model results in

$$FeS_{2-x}=\sum_{n=0}^{5}\begin{bmatrix}6\\n\end{bmatrix}\left[\frac{x}{2}\right]^n\left[1-\frac{x}{2}\right]^{6-n}FeS_{6-n} + \sum_{m=0}^{1}\begin{bmatrix}2\\m\end{bmatrix}\left[\frac{x}{2}\right]^m\left[1-\frac{x}{2}\right]^{2-m}S_{2-m}Fe_3 \ , \tag{B7}$$

with sums extending only to the molecular cells FeS_1 ($n=5$) and S_1Fe_3($m=1$) to provide that all molecules are linked to the lattice.

Table V shows the relative frequencies of FeS_{6-n} and $S_{2-m}Fe_3$ coordinations in sulfur-deficient iron pyrite, setting $P(S)=0.95$ ($FeS_{1.9}$). The table shows that although the sulfur deficit is only 5 at. % for this example, a quarter of all iron coordinations are disturbed.

These relative frequencies lay the quantitative basis for band-structure calculations that rely on the superposition of neighbored atomic wave functions. To calculate the electronic structure of sulfur-deficient pyrite properly all local coordinations have to be incorporated, and not only those of the ideal stoichiometric compound.

[1]A. Ennaoui, S. Fiechter, W. Jaegermann, and H. Tributsch, J. Electrochem. Soc. **133**, 97 (1986).
[2]A. Ennaoui, S. Fiechter, H. Goslowsky, and H. Tributsch, J. Electrochem. Soc. **132**, 1579 (1985).
[3]S. Fiechter, J. Mai, A. Ennaoui, and W. Szacki, J. Cryst. Growth **78**, 438 (1986).
[4]G. Chatzitheodorou *et al.*, Mat. Res. Bull. **21**, 1481 (1986).
[5]G. Smestad *et al.*, Sol. Energy Mat. **18**, 299 (1989).
[6]G. Smestad *et al.*, Sol. Energy Mat. **20**, 149 (1990).
[7]S. Bausch *et al.*, Appl. Phys. Lett. **57**, 25 (1990).
[8]A. Ennaoui and H. Tributsch, Sol. Cells **13**, 197 (1984).
[9]A. Ennaoui and H. Tributsch, Sol. Energy Mat. **14**, 461 (1986).
[10]R. Memming, in *Photochemistry and Photophysics,* edited by J. F. Rabek (Chemical Rubber, Cleveland, 1990), p. 157.
[11]A. Hartmann, Ph.D. thesis, Technische Universität, Berlin, 1990.
[12]J. Luck, A. Hartmann, and S. Fiechter, Z. Anal. Chem. **334**, 441 (1989).

[13]T. A. Bither, R. J. Bouchard, W. H. Cloud, P. C. Donohue, and W. J. Siemons, Inorg. Chem. **7**, 2208 (1968).
[14]W. Folkerts, G. A. Sawatzky, C. Haas, R. A. d. Groot, and F. U. Hillebrecht, J. Phys. C **20**, 4135 (1987).
[15]M. A. Kahn, J. Phys. C **9**, 81 (1976).
[16]E. K. Li, K. H. Johnson, D. E. Eastman, and J. L. Freeouf, Phys. Rev. Lett. **32**, 470 (1974).
[17]H.-M. Kühne, Ph.D. thesis, Freie Universität, Berlin, 1985.
[18]S. L. Finklea, L. Cathey, and E. L. Amma, Acta Crystallogr. A **32**, 529 (1976).
[19]M. J. Buerger, Am. Mineral. **19**, 37 (1934).
[20]F. G. Smith, Am. Mineral. **27**, 1 (1942).
[21]R. Juza, W. Biltz, and K. Meisel, Z. Anorg. Allg. Chem. **205**, 273 (1932).
[22]S. Fiechter and M. Kühne, J. Cryst. Growth **83**, 517 (1987).
[23]J. B. Goodenough and A. Hamnett, in *Zahlenwerte aus Naturwissenchaften und Technik,* edited by O. Madelung, Landolt-Börnstein (Springer, Berlin, 1984), p. 208.
[24]R. Kretz, in *Handbook of Chemistry and Physics,* edited by R. C. Weast, (Chemical Rubber, Boca Raton, 1986), p. B-186.
[25]M. F. C. Ladd and R. A. Palmer, *Structure Determination by X-ray Crystallography* (Plenum, New York, 1977).
[26]M. A. Peacock and F. G. Smith (unpublished).
[27]E. D. Stevens, M. L. DeLucia, and P. Coppens, Inorg. Chem. **19**, 813 (1979).
[28]P. Bayliss, Am. Mineral. **62**, 1168 (1977).
[29]G. Brostigen and A. Kjekshus, Acta Chem. Scand. **24**, 2993 (1970).
[30]G. Will, J. Lauterjung, H. Schmitz, and E. Hinze, in Mat. Res. Soc. Symp. **22**, 49 (1984).
[31]A. J. C. Wilson, *Mathematical Theory of X-ray Powder Diffractometry* (Philips Technical Library, Eindhoven, 1963).
[32]M. Birkholz, Ph.D. thesis, Freie Universität, Berlin, 1990.
[33]IMSL, User's Manual—Stat/Library (Fortran Subroutines for Statistical Analysis, Version 1.0) Houston, 1987.
[34]L. E. Alexander and H. P. Klug, *X-ray Diffraction Procedures for Polycrystalline and Amorphous Materials* (Wiley-Interscience, New York, 1974).
[35]R. D. Deslates and A. Henius, Phys. Rev. Lett. **31**, 972 (1973).
[36]E. R. Cohen and B. N. Taylor, Phys. Today Buyer's Guide (1989), p. 8.
[37]S. Stecura and W. J. Campbell, U. S. Bur. Mines. Rep. Invest. No. 5847, 47 (1961).
[38]K. H. Hellwege, in *Zahlenwerte und Funktionen aus Naturwissenschaft und Technik,* edited by K.-H. Hellwege, Londolt-Börnstein, Vol. 12c (Springer, Berlin, 1982) p. 294.
[39]R. S. Krishan, R. Srinivasan, and S. Devanarayanan, *Thermal Expansion of Crystals* (Pergamon, Oxford, 1976).
[40]H. Sutarno, O. Knop, and K. I. G. Reid, Can. J. Chem. **45**, 1391 (1967).
[41]M. A. Berding, A. Sher, and A.-B. Chen, J. Vac. Sci. Technol. A **5**, 3009 (1987).
[42]H. Kolell, Diploma thesis, Freie Universität, Berlin, 1990.
[43]M. L. Fearheiley (unpublished).
[44]W. Müller *et al.,* Phys. Rev. B **41**, 8624 (1990).
[45]A. K. Abass, Z. A. Ahmed, and R. E. Tahir, J. Appl. Phys. **61**, 2339 (1987).
[46]A. M. Karguppikar and A. G. Vedeshwar, Phys. Status Solidi A **109**, 549 (1988).
[47]A. A. Krivoshein, Izv. Akad. Nauk SSSR, Ser. Fiz. **23**, 175 (1987).
[48]K. Sato, J. Phys. Soc. Jpn. **53**, 1617 (1984).
[49]D. Herm (unpublished).
[50]P. Burgardt and M. S. Seehra, Solid State Commun. **22**, 153 (1977).
[51]R. Schieck, A. Hartmann, S. Fiechter, R. Könenkamp, and H. Wetzel, J. Mat. Res. **5**, 1567 (1990).
[52]E. H. Kraus and I. D. Scott, Z. Kristallogr. **44**, 153 (1908).
[53]C. T. Anderson, J. Am. Chem. Soc. **59**, 486 (1937).
[54]J. Bittner, in *Jenaer Zeiss-Jahresbericht* (Zeiss, Jena, 1950), p. 177.